On Time-Domain Two-Dimensional Site Response Analysis of Topographic Structures by BEM

Mohsen Kamalian[1], Behrouz Gatmiri[2], and Abdollah Sohrabi Bidar[3]

1. Assistant Professor, Geotechnical Engineering Research Center, International Institute of Earthquake Engineering and Seismology (IIEES), email: kamalian@dena.iiees.ac.ir
2. Associate Professor, University of Tehran and Research Director and Lecturer, Ecole Nationale des Ponts et Chaussees, Paris, France, email: gatmiri@cermes.enpc.fr
3. Ph.D. Student, Seismology Research Center, International Institute of Earthquake Engineering and Seismology (IIEES), email: sohrabi@dena.iiees.ac.ir

ABSTRACT: *In this paper, an advanced formulation of time-domain two-dimensional Boundary Element Method (BEM) for linear elastodynamics is used to carry out site response analysis of topographic structures subjected to incident P-, SV-, and Rayleigh waves. A modified set of well behaved full space two-dimensional elastodynamic convoluted kernels is presented and employed, that has a higher degree of accuracy than those presented by the previous researchers. Numerical results are presented, including cases of half-plane, canyon and ridge sections, subjected to the different body and surface waves.*

Keywords: Boundary Element Method; Time domain; Site effects; Topography effects; Site response analysis; Two-dimensional transient elastodynamic kernels; In-plane wave scattering; In-plane wave propagation; Amplification

1. Introduction

Nowadays it is well established that surface topographies can have crucial influences on damage severity and its spatial distribution during strong earthquakes. It is apparent that seismic wave scattering by topographical structures is a complex problem, which can only be solved accurately, economically and under realistic conditions, with the aid of numerical methods.

Site response analysis of topographical structures could be carried out using one of the following procedures: Domain type methods such as the Finite Element Method (*FEM*); Boundary type methods such as the Boundary Element Method (*BEM*); and Hybrid type methods, which combine the effective characteristics of two or more methods, such as the *FE*/*BE* method. Formulating the numerical procedure entirely in time domain, enables one to solve also non-linear wave propagation problems.

For domains of infinite extensions, the domain type discretization such as a FE mesh, leads to wave reflections at the edges of the mesh, which could be only partly eliminated for some cases by using the so-called transmitting, silent and non-reflecting viscous boundaries [1, 2]. Other solutions, such as the infinite element or the consistent infinitesimal *FE* cell methods, because of their important disadvantage of being formulated in transformed space, could not be used in nonlinear dynamic analysis.

The *BEM* is a very effective numerical tool for dynamic analysis of linear elastic bounded and unbounded media. The method is very attractive for wave propagation problems, because the discretization is done only on the boundary, yielding smaller meshes and systems of equations. Another advantage is that this method represents efficiently the outgoing waves through infinite domains, which is very useful when dealing with scattered waves by topographical structures. When this method is applied to problems with semi-infinite domains, there is no need to model the far field.

Regarding the time domain two-dimensional *BEM* analysis of an elastodynamic continuum, Mansur [3] and Antes [4] were the first ones who formulated a time-stepping algorithm using two-dimensional kernels. But their traction kernels were very complicated and appeared only implicitly in the *BEM* formulation. Later Israil and Banerjee [5-7] derived explicit and much simpler kernels, which could be more easily implemented in 2*D* transient elastodynamic *BEM* formulations, and used these kernels successfully in various non seismic wave propagation problems. But due to some inaccuracies in their published kernels, the convoluted kernels for constant and linear temporal variations did not reduce to the corresponding elastostatic ones at very large time steps. Kamalian [8] and Gatmiri and Kamalian [9,10] modified these two-dimensional kernels and applied them in a hybrid *FEM/BEM* dynamic analysis of non-linear saturated porous media.

Regarding two-dimensional site response analysis of topographic structures, to the best knowledge of the authors, only a few works have been done by the BEM, which were mostly done in transformed domains [11-23]. Takemiya and Fujiwara [24] used a time-domain two-dimensional *BEM* to analyse the seismic response of canyons and alluvial basins, but their formulation was restricted to the scattering of anti-plane (*SH*) waves, which involves less computational effort.

This paper presents the algorithm and the complete set of modified transient elastodynamic kernels needed for solving two-dimensional in-plane (*P* & *SV*) wave scattering problems in time domain. Demonstrating the accuracy and efficiency of the modified well behaved transient elastodynamic kernels and also demonstration of the ability to carry out site response analysis of topographical structures by this time-stepping *BEM* are the two essences of this paper.

2. Basic Equations

The governing equation for an elastic, isotropic and homogeneous body with a small amplitude displacement field can be written as:

$$\left(c_1^2 - c_2^2\right) \cdot u_{j,ij} + c_2^2 \cdot u_{i,jj} + b_i - \ddot{u}_i = 0 \tag{1}$$

in which u_i denotes the displacement vector, b_i denotes the body force vector, and c_1 and c_2 are the propagational velocities of the longitudal and transverse waves respectively which are given by $c_1^2 = (\lambda + 2\mu)/\rho; c_2^2 = \mu/\rho$, with λ and μ being the Lame constants and ρ the mass density. The corresponding governing boundary integral equation for an elastic, isotropic, homogeneous body can be obtained using the well known weighted residual method [25] as:

$$c_{ij}(\xi) \cdot u_i(\xi, t) = \int_G \left(t_i(x,t) * G_{ij} - F_{ij} * u_i(x,t)\right) \cdot dG \tag{2}$$

where G_{ij} *and* F_{ij} are the transient displacement and traction kernels, respectively, and represent the displacements and tractions at a point x at time t due to a unit point force applied at ξ and the preceding time $t = 0$. The terms $G_{ij} * t_i$ *and* $F_{ij} * u_i$ are the Riemann convolution integrals, t_i represents the traction and c_{ij} denotes the well known discontinuity term resulting from the singularity of the F_{ij} kernel. In Eq. (2), the contributions due to initial conditions and body forces are neglected. In the case of seismic loading, assuming that the total displacement can be splitted into incident ($u_i^{inc.}$) and scattered ($u_i^{sc.}$) components, the above mentioned governing boundary integral equation should be modified as follows [15-16, 23]:

$$c_{ij}(\xi) \cdot u_i(\xi, t) = \int_G \left(t_i(x,t) * G_{ij} - F_{ij} * u_i(x,t)\right) \cdot dG + u_j^{inc.}(\xi, t) \tag{3}$$

3. Time and Space Integration

Implementation of boundary integral Eqs. (2) or (3) needs approximation in both temporal and spatial variations of the field variables.

3.1 Temporal Integration

For temporal integration, the time axis is divided into N equal steps, so that $T = NDt$. Using a linear time variation of the field variables, the displacements and tractions are expressed as:

$$u_i(x, \tau) = M_1(\tau) \cdot u_i^n(x) + M_2(\tau) \cdot u_i^{n-1}(x) \tag{4a}$$

$$t_i(x, \tau) = M_1(\tau) \cdot t_i^n(x) + M_2(\tau) \cdot t_i^{n-1}(x) \tag{4b}$$

where $M_1(\tau)$ and $M_2(\tau)$ are linear temporal shape functions given by:

$T_{n-1} \prec \tau \prec T_n$:

$$M_1(\tau) = \frac{\tau - T_{n-1}}{Dt} \qquad \& \qquad M_2(\tau) = \frac{T_n - \tau}{Dt} \tag{5}$$

Subscripts 1 and 2 refer to the forward and backward temporal nodes, respectively, during a time step. Thus the time integration involves only the kernels and is expressed by:

$$\begin{aligned} G_{ij1}^{N+1-n}(r) &= \int_{(n-1)\cdot Dt}^{n\cdot Dt} G_{ij}(r, t-\tau)\cdot M_1(\tau)\cdot d\tau \\ G_{ij2}^{N+1-n}(r) &= \int_{(n-1)\cdot Dt}^{n\cdot Dt} G_{ij}(r, t-\tau)\cdot M_2(\tau)\cdot d\tau \end{aligned} \tag{6}$$

Combining this and a similar expression for the F-kernels in Eq. (2), the convoluted *BEM* equation for linear temporal variation is:

$$c_{ij}\cdot u_i^N(\xi) = \sum_{n=1}^{N}\int_G \left(\begin{bmatrix} G_{ij1}^{N+1-n}(r)\cdot t_i^n(x) + \\ G_{ij2}^{N+1-n}(r)\cdot t_i^{n-1}(x) \end{bmatrix} - \begin{bmatrix} F_{ij1}^{N+1-n}(r)\cdot u_i^n(x) + \\ F_{ij2}^{N+1-n}(r)\cdot u_i^{n-1}(x) \end{bmatrix} \right)\cdot dG \tag{7}$$

Eq. (7) can alternately be written as:

$$c_{ij}\cdot u_i^N(\xi) = \sum_{n=1}^{N}\int_G \begin{pmatrix} \left[G_{ij1}^{N+1-n}(r) + G_{ij2}^{N-n}(r)\right]\cdot t_i^n(x) \\ -\left[F_{ij1}^{N+1-n}(r) + F_{ij2}^{N-n}(r)\right]\cdot u_i^n(x) \end{pmatrix}\cdot dG \tag{8}$$

Eq. (8) has the advantage that the apparent singularity terms at the wave fronts in the F-kernels (of order $r^{-1/2}$) vanish and hence its spatial integration is straightforward.

3.2. Spatial Integration

The geometry is modelled with isoparametric quadratic elements. Using the shape functions $N_k(\eta)$ in the intrinsic co-ordinates (η) of the element, after spatial discretization, Eq. (8) transforms into:

$$c_{ij}\cdot u_i^N(\xi) = \sum_{n=1}^{N}\sum_{q=1}^{Q} \left\{ \begin{array}{l} T_{ik}^n\cdot \int_{G_q}\left[G_{ij1}^{N+1-n}(r) + G_{ij2}^{N-n}(r)\right]\cdot N_k(\eta)\cdot |J|\cdot d\eta - \\ U_{ik}^n\cdot \int_{G_q}\left[F_{ij1}^{N+1-n}(r) + F_{ij2}^{N-n}(r)\right]\cdot N_k(\eta)\cdot |J|\cdot d\eta \end{array} \right\} \tag{9}$$

where Q is the total number of boundary elements and $|J|$ is the Jacobian of transformation. It should be mentioned that the transient kernel G_{ij1}^1 and F_{ij1}^1 have the same type and order of singularity as their corresponding elastostatic kernels. The first (weak) singular integral could be accurately evaluated using the Gaussian normal quadrature rule, provided an intelligent subsegmentation with suitable mapping is adopted to make the kernel-shape function-Jacobian product well behaved over each sub-segment. The second (strong) singular integral is evaluated indirectly using the concept of rigid body motion:

$$c_{ij} + \int_{G_q} F_{ij1}^1\cdot N_k\cdot |J|\cdot d\eta = c_{ij} + \int_{G_q} F_{ij}^{static}\cdot N_k\cdot |J|\cdot d\eta + \int_{G_q}\left(F_{ij1}^1 - F_{ij}^{static}\right)\cdot N_k\cdot |J|\cdot d\eta \tag{10}$$

The diagonal 2×2 block of the assembled F_{ij1}^1 matrix contains the tensor c_{ij} as well as the first (singular) integral on the right hand side of Eq. (10). The evaluation of this diagonal block using the technique of rigid body motions is well known. The second (non-singular) integral of Eq. (10) could be easily evaluated using the Gaussian normal quadrature rule. It should be mentioned that using the technique of rigid body motion requires that the body has a closed boundary. Hence for half plane problems, the region of interest must be enclosed by fictitious boundary elements known as "enclosing elements" [5-7, 26]. Using this scheme, the sum of the first two terms on the right hand side of Eq. (10) should be evaluated by the summation of non-singular integrations of the static traction kernel F_{ij}^{static} over all the elements of the modelled boundary as well as the enclosing elements.

3.3. Solution Procedure

By sequentially writing Eq. (9) for each of the boundary nodes, the assembled system of equation takes the following matrix form:

$$\sum_{n=1}^{N}\begin{pmatrix} \left(\mathbf{G}_1^{N+1-n} + \mathbf{G}_2^{N-n}\right)\cdot\mathbf{T}^n \\ -\left(\mathbf{F}_1^{N+1-n} + \mathbf{F}_2^{N-n}\right)\cdot\mathbf{U}^n \end{pmatrix} = 0 \tag{11}$$

By transferring all known terms to the right side it becomes:

$$\mathbf{F}_1^1\cdot\mathbf{U}^N = \mathbf{G}_1^1\cdot\mathbf{T}^N + \mathbf{Z}^N \tag{12a}$$

where $\mathbf{Z}^N$ includes both effects of the past dynamic history and of the incident motion on the current time node:

$$\mathbf{Z}^N = \sum_{n=1}^{N-1}\begin{pmatrix}\left(\mathbf{G}_1^{N+1-n}+\mathbf{G}_2^{N-n}\right).\mathbf{T}^n \\ -\left(\mathbf{F}_1^{N+1-n}+\mathbf{F}_2^{N-n}\right).\mathbf{U}^n\end{pmatrix}+\mathbf{U}^{inc.N} \tag{12b}$$

Eq. (12a) can be solved for the unknown displacement values using any standard matrix solver.

4. Modified Elastodynamic Kernels

The two-dimensional full space elastodynamic kernels $G_{ij1}^{N+1-n}+G_{ij2}^{N-n}$ and $F_{ij1}^{N+1-n}+F_{ij2}^{N-n}$, which are modified versions of those proposed in reference [6, 7], are given as below:

$$G_{ij1}^{N+1-n}(r)+G_{ij2}^{N-n}(r)=\frac{1}{2\cdot\pi\cdot\rho}\cdot\sum_{k=1}^{2}\frac{1}{c_k^2}\cdot \begin{bmatrix}\frac{\delta_{ij}}{2}\cdot\begin{bmatrix}(N-n+1)\cdot\cosh^{-1}\left((N-n+1)\cdot\frac{c_k\cdot Dt}{r}\right)\\ -2\cdot(N-n)\cdot\cosh^{-1}\left((N-n)\cdot\frac{c_k\cdot Dt}{r}\right)\\ +(N-n-1)\cdot\cosh^{-1}\left((N-n-1)\cdot\frac{c_k\cdot Dt}{r}\right)\end{bmatrix}\\ +(-1)^k\cdot\frac{1}{2}\cdot\left(\delta_{ij}-2\cdot r_{,i}\cdot r_{,j}\right)\cdot\left(\frac{c_k\cdot Dt}{r}\right)^2\cdot S_k- \\ (-1)^k\cdot\frac{1}{3}\cdot\left(\delta_{ij}-2\cdot r_{,i}\cdot r_{,j}\right)\cdot\left(\frac{c_k\cdot Dt}{r}\right)^2\cdot Q_k- \\ (-1)^k\cdot\left(\delta_{ij}\cdot\delta_{2k}-r_{,i}\cdot r_{,j}\right)\cdot P_k\end{bmatrix} \tag{13a}$$

$$F_{ij1}^{N+1-n}(r)+F_{ij2}^{N-n}(r)=$$

$$\frac{\mu}{2\cdot\pi\cdot\rho\cdot r}\cdot\sum_{k=1}^{2}\begin{bmatrix}\left\{\frac{-A_1\cdot\delta_{1k}+A_3\cdot\delta_{2k}}{c_k^2}\right\}\cdot P_k\\ -\frac{2}{3}\cdot(-1)^k\cdot A_2\cdot\left(\frac{Dt}{r}\right)^2\cdot Q_k\end{bmatrix} \tag{13b}$$

The coefficients P_k, Q_k and S_k are defined as:

$$P_k=\begin{pmatrix}\sqrt{(N-n+1)^2-\left(\frac{r}{c_k\cdot Dt}\right)^2}\\ -2\cdot\sqrt{(N-n)^2-\left(\frac{r}{c_k\cdot Dt}\right)^2}\\ +\sqrt{(N-n-1)^2-\left(\frac{r}{c_k\cdot Dt}\right)^2}\end{pmatrix} \tag{14a}$$

$$Q_k=\begin{pmatrix}\left\{(N-n+1)^2-\left(\frac{r}{c_k\cdot Dt}\right)^2\right\}^{\frac{3}{2}}\\ -2\cdot\left\{(N-n)^2-\left(\frac{r}{c_k\cdot Dt}\right)^2\right\}^{\frac{3}{2}}\\ +\left\{(N-n-1)^2-\left(\frac{r}{c_k\cdot Dt}\right)^2\right\}^{\frac{3}{2}}\end{pmatrix} \tag{14b}$$

$$S_k=\begin{pmatrix}(N-n+1)^2\cdot\sqrt{(N-n+1)^2-\left(\frac{r}{c_k\cdot Dt}\right)^2}\\ -2\cdot(N-n)^2\cdot\sqrt{(N-n)^2-\left(\frac{r}{c_k\cdot Dt}\right)^2}\\ +(N-n-1)^2\cdot\sqrt{(N-n-1)^2-\left(\frac{r}{c_k\cdot Dt}\right)^2}\end{pmatrix} \tag{14c}$$

and the coefficients A_1, A_2 and A_3 are given as:

$$A_1=(\lambda/\mu)\cdot n_i\cdot r_{,j}+2\cdot r_{,i}\cdot r_{,j}\cdot\frac{\partial r}{\partial n}$$

$$A_2=n_i\cdot r_{,j}+n_j\cdot r_{,i}+\frac{\partial r}{\partial n}\cdot\left(\delta_{ij}-4\cdot r_{,i}\cdot r_{,j}\right) \tag{15}$$

$$A_3=\frac{\partial r}{\partial n}\cdot\left(2\cdot r_{,i}\cdot r_{,j}-\delta_{ij}\right)-n_j\cdot r_{,i}$$

In evaluating the above terms the causality condition must always be satisfied, i.e. the time-related terms can not be negative. Because the contribution to each of the longitudal and transverse waves is null, if the wave has not reached the field point.

It should be mentioned that in Israil and Banerjee's proposed expressions for the above mentioned transient kernels [5-7], the third term of Eq. (13a) lacked the coefficient $(c_k.Dt/r)^2$ and the second term of Eq. (13b) lacked the coefficient (2/3). As indicated in references 5 to 7, at very large time steps, the convoluted transient kernels (for $N = n = 1$) should reduce to their corresponding elastostatic ones. Table (1) compares the limit values of Israil and Banerjee's convoluted traction kernels [6, 7] at very large time steps with those evaluated by Eq. (13), for a medium with shear modulus of 900*Mpa*, Poisson ratio of 1/3 and mass density of 2.00t/m^3. The source is located at (2, 0), the quadratic element consists of nodes (4, 2), (3, 3) and (2, 4), and the receiver is located at (3, 3). As can be seen, Israil and Banerjee's convoluted traction kernels [6, 7] do not reduce to their corresponding elastostatic ones, whereas those evaluated by Eq. (13) do. The elastodynamic kernels $G_{ij1,2}^{N+1-n}$ and $F_{ij1,2}^{N+1-n}$ which are modified versions of those proposed in reference [5] are given in Appendix (I).

Table 1. Convoluted traction kernels at large time steps.

References	$F_{ij1}^{N+1-n} + F_{ij2}^{N-n}$ ($*$ -10^{-2})			
	1--1	**1--2**	**2--1**	**2--2**
Elastostatic [25]	1.81	2.59	1.44	7.19
Eq. (13)	1.81	2.59	1.45	7.19
Israil & Banerjee	-0.034	1.78	2.92	9.04

5. Numerical Applications

The above formulation has been implemented in a general purpose two-dimensional nonlinear two-phase *BEM/FEM* code named as *HYBRID* [8-10]. Problems can be solved either by *BEM*, *FEM* or a combination of them. The numerical examples of this section are designed to demonstrate the accuracy and efficiency of the modified well behaved two-dimensional transient elastodynamic kernels and also the ability to carry out site response analysis of topographical structures by the presented time-stepping *BEM*.

5.1. Free Field Motion of Half-Space

The purpose of this example is to illustrate the applicability and accuracy of the presented *BEM* formulation in performing site response analysis of linear elastic regular unbounded regions. Figure (1) shows the geometry used for the solution of a

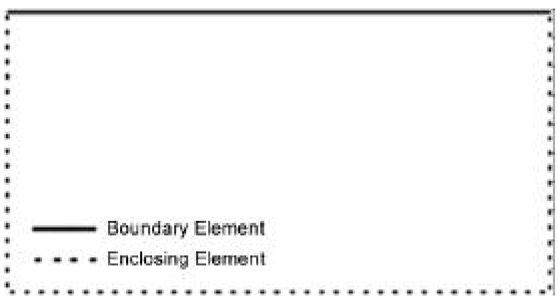

Figure 1. BEM idealization of the half-plane.

homogeneous half-plane subjected to vertical propagating harmonic incident *SV* and *P* waves with a predominant frequency of 1.59*Hz* and maximum amplitude of 0.001*m*. The shear wave velocity of the medium is 223.3m/s, its Poisson ratio is 1/3 and its mass density is 2.00t/m^3. 35 quadratic boundary elements were used in order to discretize the free surface. Figure (2) compares the horizontal displacement time history obtained at the ground surface with the analytically obtained free field motion [27], in the case of *SV*-type incident wave. As can be seen, there exists an excellent agreement between the obtained results. The figure also shows that as expected, the vertical displacement is zero. The same results with horizontal and vertical displacements inter-changed in Figure (2) are obtained, when the case of *P*-type incident wave is considered.

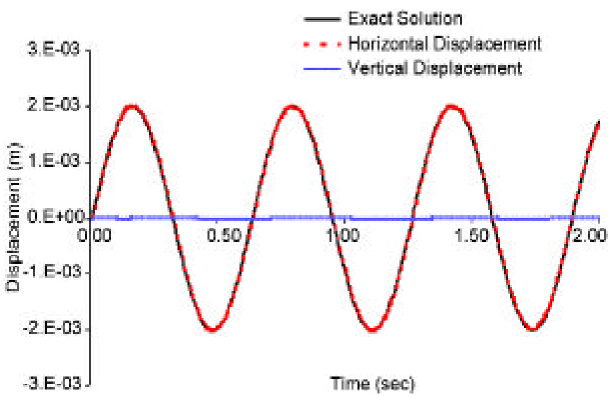

Figure 2. Analytical and numerical obtained free field motions in the case of the SV incident wave.

5.2. Semi Circular Shaped Canyon

The purpose of this example is to illustrate the applicability and accuracy of the presented *BEM* formulation in performing site response analysis of canyon structures. Figure (3) shows a semi circular canyon subjected to vertically propagating *SV* and *P* waves of the Ricker type:

$$f(t) = \left[1 - 2 \cdot (\pi \cdot f_p \cdot (t - t_0))^2\right] e^{-(\pi \cdot f_p \cdot (t - t_0))^2}$$

f_p and t_0 denote the predominant frequency and an appropriate time shift parameter, respectively. This problem was studied in a dimensionless form by Wong [11], Dravinski and Mossessian [12], Mossessian and Dravinski [13], Kawase [15] and Sanchez-Sesma and Campillo [17] for purely elastic or weakly inelastic media. The canyon has a radius of *(r)*, a shear wave velocity of (c_2) and a Poisson's ratio of 1/3. The problem is solved using 123 quadratic elements and the results are demonstrated as spectral amplifications versus normalized frequencies $(W = \omega r / \pi c_2)$.

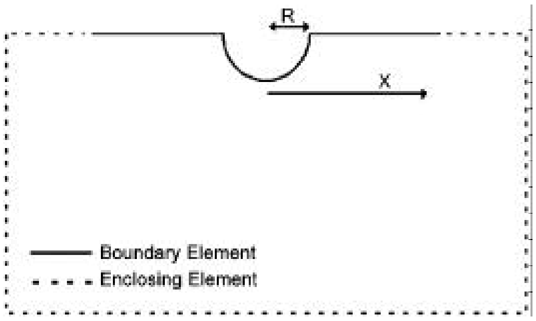

Figure 3. Geometry and discretization of the semi circular canyon and the half-plane.

Figure (4) compares the spectral amplifications obtained in the present study with those obtained by Wong [11], Dravinski and Mossessian [12] and Mossessian and Dravinski [13] for a normalized frequency of 0.5. As can be seen, in both cases of *SV* and *P* waves, there exist an excellent agreement for both vertical and horizontal components. Figure (5) too, compares the spectral amplifications obtained in the present study with those obtained by Wong [11], Kawase [15] and Sanchez-Sesma & Campillo [17] for a normalized frequency of 2.0. There exist too, in both cases of *SV* and *P* waves, an excellent agreement for both vertical and horizontal components.

5.3. Semi Sine Shaped Ridge

The purpose of this example is to illustrate the applicability and accuracy of the presented *BEM* formulation in performing site response analysis of ridge structures. A long semi-sine shaped cross section ridge, as shown in Figure (6) is subjected to the vertically propagating Ricker type *SV* wave of Figure (7). The Ricker wave has a predominant frequency of 3*Hz* and maximum amplitude of 1*mm*. The ridge is symmetric with a half width of 200*m* and a height of 100*m*. The shear wave velocity is 800*m/s*, the Poisson ratio is 1/3 and the mass density is 2.22t/m^3. The problem is solved twice using two methods: Once with the

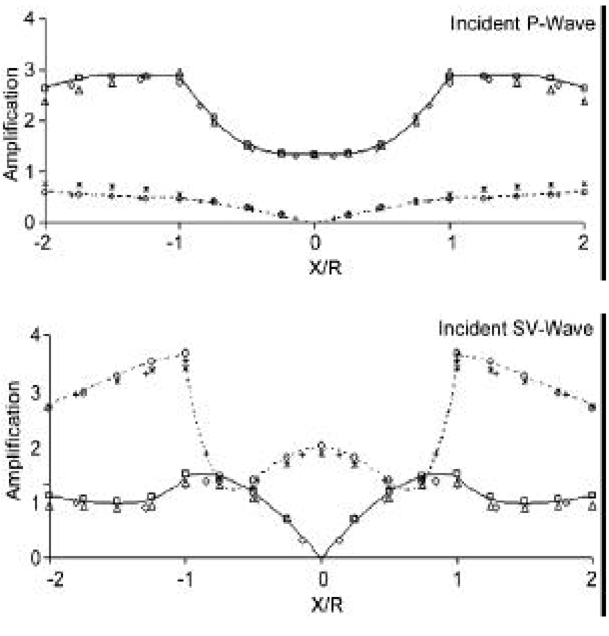

Figure 4. Amplification of surface displacements for a semi circular canyon in the case of W =0.5. The solid and dashed lines represent the vertical and horizontal components of the present study. The triangle and star symbols represent the vertical and horizontal components obtained by Wong [11] respectively. The square and circle symbols represent the vertical and horizontal components obtained by Dravinski and Mossessian [12] respectively. The lozenge and plus symbols represent the vertical and horizontal components obtained by Mossessian and Dravinski [13] respectively.

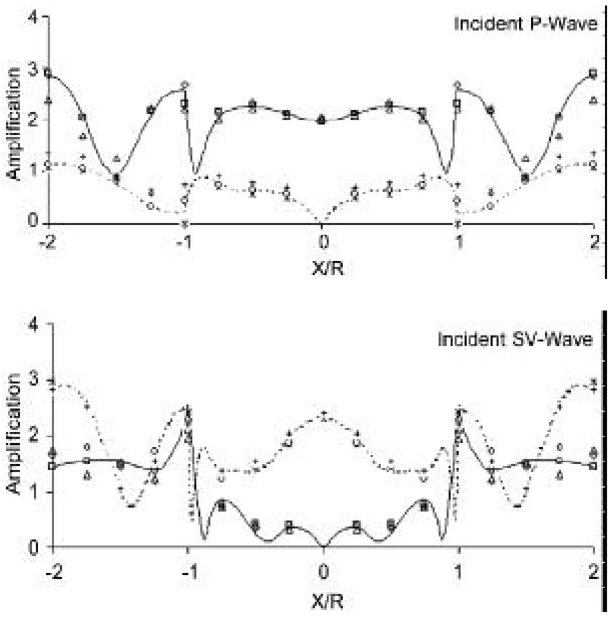

Figure 5. Amplification of surface displacements for a semi circular canyon in the case of $W = 2.0$. The solid and dashed lines represent the vertical and horizontal components of the present study. The triangle and star symbols represent the vertical and horizontal components obtained by Wong [11] respectively. The square and circle symbols represent the vertical and horizontal components obtained by Sanches-Sesma and Campillo [17] respectively. The lozenge and plus symbols represent the vertical and horizontal components obtained by Kawase [15] respectively.

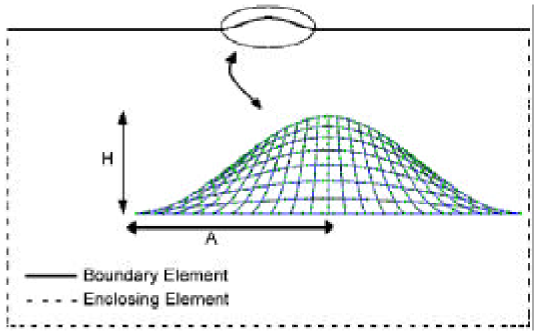

Figure 6. Geometry and discretization of the semi sine shaped ridge and the half-plane.

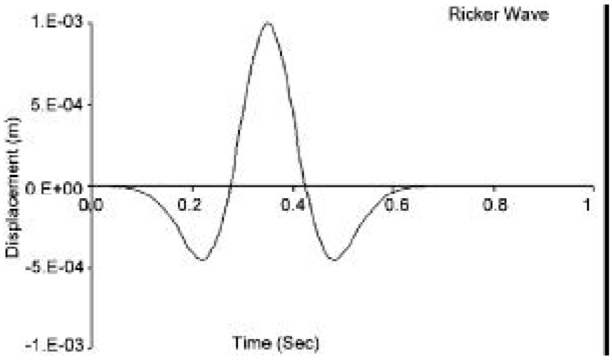

Figure 7. Incident Ricker type motion.

BE method and once with a hybrid *BE/FE* method. In the first case 178 quadratic boundary elements and in the second case 140 eight nodded cubic finite elements and 164 quadratic boundary elements were used. Figures (8) and (9) compare the obtained displacements at top and base of the ridge respectively. As can be seen, there exists a very good agreement between the obtained results.

5.4. Surface Loaded Elastic Half-Plane

The purpose of this example is to demonstrate the ability of the presented *BEM* formulation to show generation of Rayleigh waves in a loaded elastic half-plane. The analytical treatment of the problem was given by Lamb [28]. The elastic half-plane shown in Figure (10) is loaded with a stress field, the spatial and temporal variations of which are triangular. The triangular spatial distribution is chosen to simulate a line load (in 2*D*) while the triangular pulse simulates a delta pulse time. The discretization is extended up to a distance of 22b, where *b* is the half-width of the loaded area. 24 quadratic elements are used in order to discretize the free surface. The

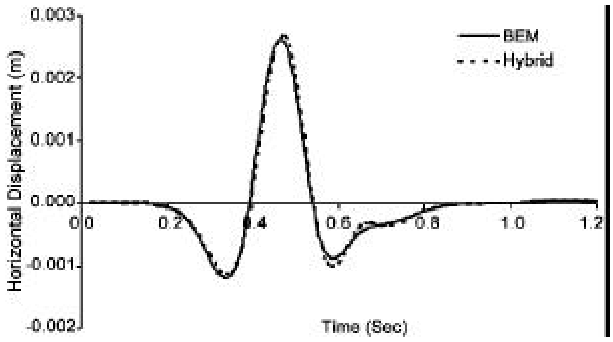

Figure 8. Horizontal displacement at the top of the ridge: comparison of BEM and hybrid results.

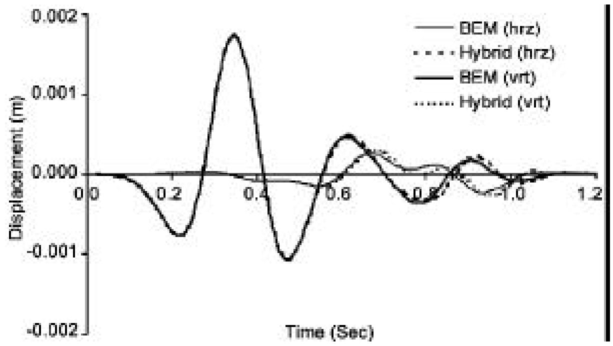

Figure 9. Horizontal and vertical displacement at the base of the ridge: comparison of BEM and hybrid results.

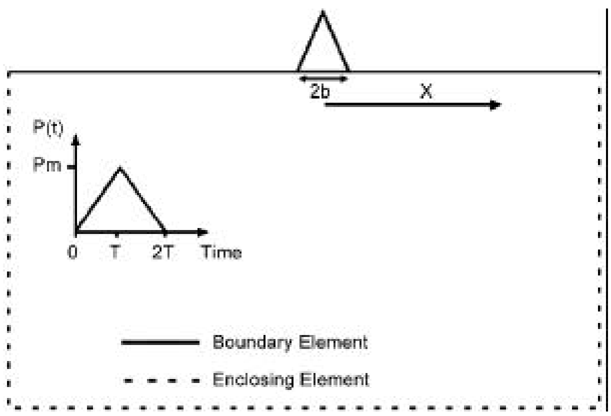

Figure 10. BEM idealization of the loaded half-plane.

region has a modulus of elasticity *of E*=330*Mpa*, a Poisson's ratio of $\nu = 0.25$ and a mass density 2.04t/m^3. The maximum load intensity is 100*Kpa* and its duration is 0.02 second.

Figure (11) shows the vertical and horizontal displacements of point *A* (3b,0) on the free surface, obtained by the present formulation using two different time steps. Excellent agreement is noticed between the results. The normalized horizontal and

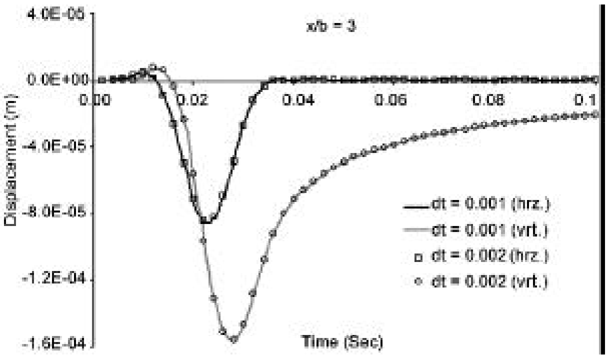

Figure 11. Calculated displacements at point *A* (Two different time-steps).

vertical displacements of points *A*, *B* (6b,0) and *C* (9b,0) are compared to each other in Figures (12) and (13) respectively. The normalized displacements are obtained by multiplying the corresponding displacement components by $\pi.\mu.x/(2.c_2.Q)$, where Q denote the magnitude of the triangular pulse. The normalized time is defined by $c_2.t/b$. As expected, Figures (12) and (13) show that as the point is farther away from the loaded region, the results converge towards Lamb's solution [28], indicating that with increasing distance, the load appears to be a point load.

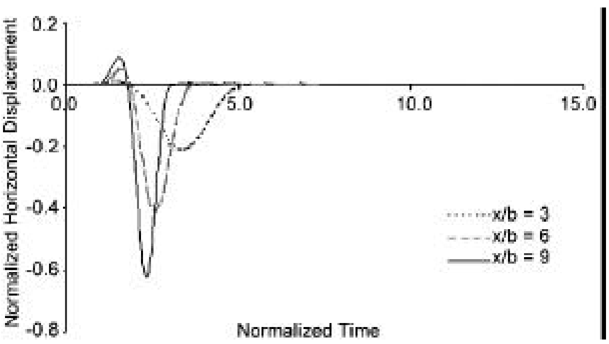

Figure 12. Normalized horizontal displacements at the free surface.

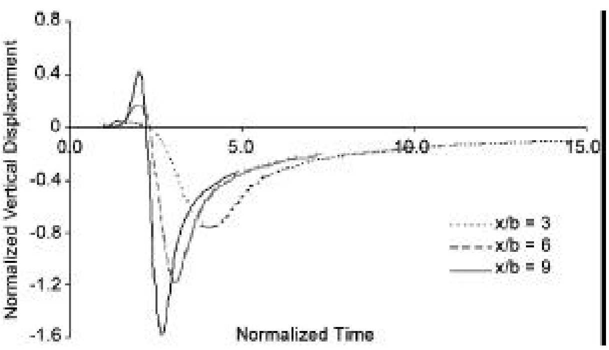

Figure 13. Normalized vertical displacements at the free surface.

6. Conclusion

In this paper it is shown that the advanced time stepping *BEM* could be used in order to perform transient two-dimensional site response analysis of topographic structures. A modified set of full-space transient two-dimensional elastodynamic kernels is presented and applied. The accuracy, efficiency and applicability of the formulation are demonstrated through a number of numerical transient in-plane wave scattering examples. The presented algorithm can be easily combined with the finite element method in order to carry out site response analysis of nonlinear media.

References

1. Lysmer, J. and Kuhlemeyer, R.L. (1969). "Finite Dynamic Model for Infinite Media", *J. of Engineering Mechanics*, *ASCE*, **EM4**, 859-877.

2. White, W., Valliappan, S., and Lee, I.K. (1977). "Unified Boundary for Finite Dynamic Models", *J. of Engineering Mechanics, ASCE*; **103**(5), 969-964.

3. Mansur, W.J. (1983). "A Time-Stepping Technique to Solve Wave Propagation Problems Using the Boundary Element Method", Ph.D. Dissertation, Southampton University.

4. Antes, H. (1985). "A Boundary Element Procedure for Transient Wave Propagation in Two-Dimensional Isotropic Elastic Media", Finite Element Anal. Des., **1**, 313-322.

5. Israil, A.S.M. and Banerjee, P.K. (1990a). "Advanced Time Domain Formulation of BEM for Two-Dimensional Transient Elastodynamics", *Int. J. for Num. Methods in Eng.*, **29**, 1421-1440.

6. Israil, A.S.M. and Banerjee, P.K. (1990b). "Two-Dimensional Transient Wave Propagation by Time Domain BEM", *Int. J. Solids and Structures*, **26**(8), 851-864.

7. Israil, A.S.M. and Banerjee, P.K. (1992). "Advanced Development of Boundary Element Method for Two-Dimensional Dynamic Elasto-Plasticity", *Int. J. Solids and Structures*, **29**(11), 1433-1451.

8. Kamalian, M. (2001). "Time Domain Two-Dimensional Hybrid FEM/BEM Dynamic Analysis

of Non-Linear Saturated Porous Media", Ph.D. Dissertation, Tehran University.

9. Gatmiri, B. and Kamalian, M. (2002a). "Time Domain Two-Dimensional Hybrid FEM/BEM Dynamic Analysis of Non-Linear Saturated Porous Media", *2nd Canadian Speciality Conf. on Computing in Geotechnique*.

10. Gatmiri, B. and Kamalian, M. (2002b). "Combination of Boundary Element and Finite Element Methods for Evaluation of Dynamic Response of Saturated Porous Media", *5th European Conference on Numerical Methods in Geotechnical Engineering*.

11. Wong, H.L. (1982). "Effects of Surface Topography on the Diffraction of P, SV and Rayleigh Waves", *Bull. Seismol. Soc. Am.*, **72**, 1167-1183.

12. Dravinski, M. and Mossessian, T.K. (1987). "Scattering of Plane Harmonic P, SV, and Reyleigh Waves by Dipping Layers of Arbitrary Shape", *Bull. Seismol. Soc. Am.*, **77**, 212 – 235.

13. Mossessian, T.K. and Dravinski, M. (1987). "Application of a Hybrid Method for Scattering of P, SV, and Reyleigh Waves by Near-Surface Irregularities", *Bull. Seismol. Soc. Am.*, **77**, 1784-1803.

14. Kawase, H. (1987). "Irregular Ground Analysis to Interpret Time Characteristics of Strong Ground Motion Recorded in Mexico City During 1985 Mexico Earthquake", In "Ground Motion and Engineering Seismology", Ed. Cakmak A.S., Development in Geotechnical Engineering, **44**, Elsevier, Amsterdam, 467-476.

15. Kawase, H. (1988). "Time-Domain Response of a Semi-Circular Canyon for Incident P, SV and Rayleigh Waves Calculated by the Discrete Wavenumber Boundary Element Method", *Bull. Seismol. Soc. Am.*, **78**, 1415-1437.

16. Kawase, H. and Aki, K. (1989). "A Study of the Response of a Soft Basin for Incident S, P and Rayleigh Waves with Special Reference to the Long Duration Observed in Mexico City", *Bull. Seismol. Soc. Am.*, **79**, 1361-1382.

17. Sanchez-Sesma, F.J. and Campillo, M. (1991). "Diffraction of P, SV and Rayleigh Waves by Topographic Features: A Boundary Integral Formulation", *Bull. Seismol. Soc. Am.*, **81**, 2234-2253.

18. Sanchez-Sesma, F.J. and Campillo, M. (1993). "Topographic Effects for Incident P, SV and Rayleigh Waves", *Tectonophysics*; **218**, 113-125.

19. Sanchez-Sesma, F.J. and Luzon, F. (1995). "Seismic Response of Three Dimensional Alluvial Valleys for Incident P, SV and Rayleigh Waves", *Bull. Seismol. Soc. Am.*, **85**, 269-284.

20. Papageorgiou, A.S. and Kim, J. (1993). "Propagation and Amplification of Seismic Waves in 2D Valleys Excited by Obliquely Incident P- and SV-Waves", *Int. J. Earthquake Engineering and Structural Dynamic*, **22**, 167-182.

21. Pedersen, H.A., Sanchez-Sesma, F.J., and Campillo, M. (1991). "Three-Dimensional Scattering by Two-Dimensional Topographies", *Bull. Seismol. Soc. Am.*, **84**, 1169-1183.

22. Reinoso, E., Wrobel, L.C., and Power, H. (1997). "Two-Dimensional Scattering of P, SV and Rayleigh Waves: Preliminary Results for the Valley of Mexico", *Int. J. Earthquake Engineering and Structure Dynamic*, **26**, 595-616.

23. Hadely, P.K., Askar, A., and Cakmak, A.S. (1989). "Scattering of Waves by Inclusions in a Nonhomogeneous Elastic Half Space Solved by Boundary Element Methods", Technical Report NCEER-89-0027.

24. Takemiya, H. and Fujiwara, A. (1994). "SH-Wave Scattering and Propagation Analysis at Irregular Sites by Time Domain BEM", *Bull. Seism. Soc. Am.*, **84**, 1443-1455.

25. Brebbia, C.A. and Dominguez, J. (1989). "Boundary Elements, an Introductory Course", Computational Mechanics Publications, Southampton, Boston.

26. Ahmad, S. and Banerjee, P.K. (1988). "Multi-Domain BEM for Two-Dimensional Problems of Elastodynamics", *International Journal for Numerical Methods in Engineering*, **26**, 891-911.

27. Wolf, J.P. (1985). Dynamic Soil-Structure Interaction, Prentice Hall.

28. Lamb, H. (1904). "On the Propagation of Tremors Over the Surface of an Elastic Solid", Phil. Trans. R. Soc., London, Series A203, 1-42.

Appendix I- Other Elastodynamic Kernels

The elastodynamic kernels $G_{ij1,2}^{N+1-n}$ and $F_{ij1,2}^{N+1-n}$ (Eqs. (6) and (7)) which are the modified versions of those proposed in reference [5] are given as below:

$$G_{ij1}^{N+1-n}(r)=\frac{1}{2\cdot\pi\cdot\rho}\cdot\left[\begin{array}{l}\dfrac{H(\alpha_1-1)}{c_1^2}\cdot\\ \left\{\begin{array}{l}(N-n+1)\cdot\left[\begin{array}{l}\dfrac{\delta_{ij}}{2}\cdot cosh^{-1}(\alpha_1)-\alpha_1\cdot\beta_1\\ +r_{,i}\cdot r_{,j}\cdot\alpha_1\cdot\beta_1\end{array}\right]+\\ \dfrac{r}{c_1\cdot Dt}\cdot\left[\dfrac{\delta_{ij}}{3}\cdot\beta_1^3-r_{,i}\cdot r_{,j}\cdot\left(\dfrac{2}{3}\cdot\beta_1^3+\beta_1\right)\right]\end{array}\right\}+\\ \dfrac{H(\alpha_2-1)}{c_2^2}\cdot\\ \left\{\begin{array}{l}(N-n+1)\cdot\left[\begin{array}{l}\dfrac{\delta_{ij}}{2}\cdot cosh^{-1}(\alpha_2)+\alpha_2\cdot\beta_2\\ -r_{,i}\cdot r_{,j}\cdot\alpha_2\cdot\beta_2\end{array}\right]+\\ \dfrac{r}{c_2\cdot Dt}\cdot\left[\begin{array}{l}-\dfrac{\delta_{ij}}{3}\cdot\left(\beta_2^3+3\cdot\beta_2\right)+\\ r_{,i}\cdot r_{,j}\cdot\left(\dfrac{2}{3}\cdot\beta_2^3+\beta_2\right)\end{array}\right]\end{array}\right\}\end{array}\right]_{z=(N-n)\cdot Dt}^{z=(N-n+1)\cdot Dt} \quad \text{(A-1)}$$

$$G_{ij2}^{N+1-n}(r)=\frac{1}{2\cdot\pi\cdot\rho}\cdot\left[\begin{array}{l}\dfrac{H(\alpha_1-1)}{c_1^2}\cdot\\ \left\{\begin{array}{l}(n-N)\cdot\left[\begin{array}{l}\dfrac{\delta_{ij}}{2}\cdot \cosh^{-1}(\alpha_1)-\alpha_1\cdot\beta_1\\ +r_{,i}\cdot r_{,j}\cdot\alpha_1\cdot\beta_1\end{array}\right]-\\ \dfrac{r}{c_1\cdot Dt}\cdot\left[\dfrac{\delta_{ij}}{3}\cdot\beta_1^3-r_{,i}\cdot r_{,j}\cdot\left(\dfrac{2}{3}\cdot\beta_1^3+\beta_1\right)\right]\end{array}\right\}+\\ \dfrac{H(\alpha_2-1)}{c_2^2}\cdot\\ \left\{\begin{array}{l}(n-N)\cdot\left[\begin{array}{l}\dfrac{\delta_{ij}}{2}\cdot \cosh^{-1}(\alpha_2)+\alpha_2\cdot\beta_2\\ -r_{,i}\cdot r_{,j}\cdot\alpha_2\cdot\beta_2\end{array}\right]-\\ \dfrac{r}{c_2\cdot Dt}\cdot\left[\begin{array}{l}-\dfrac{\delta_{ij}}{3}\cdot\left(\beta_2^3+3\cdot\beta_2\right)+\\ r_{,i}\cdot r_{,j}\cdot\left(\dfrac{2}{3}\cdot\beta_2^3+\beta_2\right)\end{array}\right]\end{array}\right\}\end{array}\right]_{z=(N-n)\cdot Dt}^{z=(N-n+1)\cdot Dt} \quad \text{(A-2)}$$

$$F_{ij1}^{N+1-n}(r)=\frac{\mu}{2\cdot\pi\cdot\rho\cdot r}\cdot\left[\begin{array}{l}\dfrac{H(\alpha_1-1)}{c_1^2}\cdot\\ \left\{\begin{array}{l}(N-n+1)\cdot\left[-\dfrac{\alpha_1}{\beta_1}\cdot A_1+2\cdot\alpha_1\cdot\beta_1\cdot A_2\right]+\\ \dfrac{r}{c_1\cdot Dt}\cdot\left[\dfrac{1}{\beta_1}\cdot A_1-2\cdot A_2\cdot\left(\dfrac{2}{3}\cdot\beta_2^3+\beta_2\right)\right]\end{array}\right\}+\\ \dfrac{H(\alpha_2-1)}{c_2^2}\cdot\\ \left\{\begin{array}{l}(N-n+1)\cdot\left[\dfrac{\alpha_2}{\beta_2}\cdot A_3-2\cdot\alpha_2\cdot\beta_2\cdot A_2\right]+\\ \dfrac{r}{c_2\cdot Dt}\cdot\left[-\dfrac{1}{\beta_2}\cdot A_3+2\cdot A_2\cdot\left(\dfrac{2}{3}\cdot\beta_2^3+\beta_2\right)\right]\end{array}\right\}\end{array}\right]_{z=(N-n)\cdot Dt}^{z=(N-n+1)\cdot Dt} \quad \text{(A-3)}$$

$$F_{ij2}^{N+1-n}(r)=\frac{\mu}{2\cdot\pi\cdot\rho\cdot r}\cdot\left[\begin{array}{l}\dfrac{H(\alpha_1-1)}{c_1^2}\cdot\\ \left\{\begin{array}{l}(n-N)\cdot\left[-\dfrac{\alpha_1}{\beta_1}\cdot A_1+2\cdot\alpha_1\cdot\beta_1\cdot A_2\right]-\\ \dfrac{r}{c_1\cdot Dt}\cdot\left[\dfrac{1}{\beta_1}\cdot A_1-2\cdot A_2\cdot\left(\dfrac{2}{3}\cdot\beta_2^3+\beta_2\right)\right]\end{array}\right\}+\\ \dfrac{H(\alpha_2-1)}{c_2^2}\cdot\\ \left\{\begin{array}{l}(n-N)\cdot\left[\dfrac{\alpha_2}{\beta_2}\cdot A_3-2\cdot\alpha_2\cdot\beta_2\cdot A_2\right]-\\ \dfrac{r}{c_2\cdot Dt}\cdot\left[-\dfrac{1}{\beta_2}\cdot A_3+2\cdot A_2\cdot\left(\dfrac{2}{3}\cdot\beta_2^3+\beta_2\right)\right]\end{array}\right\}\end{array}\right]_{z=(N-n)\cdot Dt}^{z=(N-n+1)\cdot Dt} \quad \text{(A-4)}$$

The coefficients α_k and β_k are given as:

$$\alpha_k = \frac{c_k \cdot z}{r} \quad \& \quad \beta_k = \sqrt{\alpha_k^2 - 1}; \quad k = 1, 2$$

Appendix II- Notation

The following symbols are used in this paper:

t_i	Traction Components
u_i	Displacement
b_i	Total Body Force
?	Mass Density
$c_{1,2}$	Longitudinal and Transverse Wave Velocities
? and μ	Lame Coefficients
r	Distance between Source and Receiver
t, ? t	Time, Time Increment
N^m	Shape Functions of Element (m)
$M_1(t)$ and $M_2(t)$	Linear Temporal Shape Functions
G_{ij} and F_{ij}	Elastodynamic Fundamental Solutions
$G_{ij1}^{N+1-n} + G_{ij2}^{N-n}$ and $F_{ij1}^{N+1-n} + F_{ij2}^{N-n}$	Elastodynamic Convoluted Transient Kernels
$\mathbf{G}_1^{N+1-n} + \mathbf{G}_2^{N-n}$ and $\mathbf{F}_1^{N+1-n} + \mathbf{F}_2^{N-n}$	Elastodynamic Kernel Tensors
$\mathbf{U}^{t+?t}$	Displacement Vector at Time t+ ? t